CrossMark

A new dynamic six degrees of freedom disc-loading simulator allows to provoke disc damage and herniation

Hans-Joachim Wilke[1] · Annette Kienle[2] · Sebastian Maile[1] · Volker Rasche[3,4] ·
Nikolaus Berger-Roscher[1]

Abstract

Purpose The cause of disc herniation is not well understood yet. It is assumed that heavy lifting and extreme postures can cause small injuries starting either in the inner anulus or from the outside close to the endplate. Such injuries are accumulated over years until its structure is weakened and finally a single loading event leads to a sudden failure of the last few intact lamellae. This paper describes a novel, custom-developed dynamic 6-DOF disc-loading simulator that allows complex loading to provoke such disc damage and herniations.

Methods The machine's axes are driven by six independent servomotors providing high loads (10 kN axial compression, 2 kN shear, 100 Nm torque) up to 5 Hz. A positional accuracy test was conducted to validate the machine. Subsequently, initial experiments with lumbar ovine motion segments under complex loading were performed. After testing, the discs were examined in an ultra-high field MRI (11.7 T). A three-dimensional reconstruction was performed to visualise the internal disc lesions.

Results Validation tests demonstrated positioning with an accuracy of $\leq 0.08°/\leq 0.026$ mm at 0.5 Hz and $\leq 0.27°/\leq 0.048$ mm at 3.0 Hz with amplitudes of $\pm 17°/\pm 2$ mm. Typical failure patterns and herniations could be provoked with complex asymmetrical loading protocols. Loading with axial compression, flexion, lateral bending and torsion lead in 8 specimens to 4 herniated discs, two protrusions and two delaminations. All disc failures occurred in the posterior region of the disc.

Conclusion This new dynamic disc-loading simulator has proven to be able to apply complex motion combinations and allows to create artificial lesions in the disc with complex loading protocols. The aim of further tests is to better understand the mechanisms by which disc failure occurs at the microstructural level under different loading conditions. Visualisation with ultra-high field MRI at different time points is a promising method to investigate the gradual development of such lesions, which may finally lead to disc failure. These kinds of experiments will help to better investigate the mechanical failure of discs to provide new insights into the initiation of intervertebral disc herniation. This device will also serve for many other applications in spine biomechanics research.

Keywords Dynamic spine tester · Disc-loading simulator · 6-DOF · Intervertebral disc · Complex loading · Herniation · Endplate junction failure

✉ Hans-Joachim Wilke
   hans-joachim.wilke@uni-ulm.de

   Annette Kienle
   annette.kettler@spineserv.de

   Sebastian Maile
   sebastian.maile@gmx.de

   Volker Rasche
   volker.rasche@uni-ulm.de

   Nikolaus Berger-Roscher
   nikolaus.berger-roscher@uni-ulm.de

[1] Institute of Orthopedic Research and Biomechanics, Center of Musculoskeletal Research (zmfu), Helmholtzstraße 14, 89081 Ulm, Germany

[2] SpineServ GmbH and Co. KG, Söflinger Straße 100, 89077 Ulm, Germany

[3] Department of Internal Medicine II, University Hospital Ulm, Albert-Einstein-Allee 23, 89081 Ulm, Germany

[4] Small Animal MRI, Medical Faculty, Ulm University, Albert-Einstein-Allee 11, 89081 Ulm, Germany

Introduction

The spinal column is an integral part of the human body allowing trunk flexibility. The spine is subject to normal age related process but also to certain disorders such as degenerative disc disease (DDD, accelerated aging) and disc prolapse [1]. The prevalence of a disc prolapse increases with age, occurring in 1–3 % of the population, and is highest in the age group 30–60 years. Incidence of prolapse is highest in the lower lumbar or lumbosacral spine (>90 %) [2–4]. This region is subjected to high biomechanical loads, which presumably account for the development of disc prolapse [1, 5]. It is still debated whether DDD leads to or protects against disc herniation [1]. There is also debate as to whether they are even interconnected [6].

Since the 1950s several studies have investigated the failure mechanism of the intervertebral disc covering the whole range from quasi-static pure compression to more complex cyclic loading situations: The first pioneers were Virgin [7], Hirsch [8], Brown et al. [9], Hardy et al. [10], and Roaf [11], followed by Farfan et al. [12] and Lin et al. [13] in the 1970s using uniaxial testing devices. In the 1980s, Wilder et al. [14, 15], Liu et al. [16, 17], as well as Adams and Hutton [18–22], further improved the testing techniques using special fixture designs that allowed combinations of compression with torsion or flexion with lateral bending. Later tests by Callaghan and McGill [23] included a second dynamic axis, e.g., used for flexion/extension. Regarding all aforementioned tests, dynamic loads were applied to a maximum of two degrees of freedom (DOF). In a study by Drake et al. [24] in addition to the dynamic loads of two DOF a static load is applied to a tertiary DOF.

It was shown that loading rate and complex loading condition greatly influence the mode of failure of the intervertebral disc [25–27]. However, existing test apparatuses are either designed for a maximum of two independently controlled DOF with high loading rates [23] or six DOF with low loading rates which allow quasi-static flexibility measurements of spinal motion segments [28–38]. Only two dynamic systems with six DOF are known to the authors: a robotic system by Fujie et al. [39], later used for spinal segments by Hurschler et al. [40] and a hexapod system by Ding et al. [41], designed to be suitable for all biomechanical joints and tissues, including spine [42]. The robotic system (KR 16, Kuka Robotik GmbH, Gersthofen, Germany) used by [40] is able to achieve very rapid motion ranging from 156 to 614°/s depending on the axis, while loads are limited to about 160 N. The custom designed hexapod system by Ding et al. [41] is capable of very high loads (up to 21 kN and 2.5 kNm). The only limitation is the

movement speed, which is between 60°/s (lateral bending) and 135°/s (axial rotation).

The cause of disc herniation is still not well understood. It is assumed that heavy lifting and extreme postures can cause small injuries starting in the inner anulus [22]. Such injuries are accumulated over years until its structure is weakened and finally a single loading event leads to a sudden failure of the last few intact lamellae. However, finite element studies suggest that complex loading also leads to high shear strain [43]. Therefore, failure may also start from the outside close to the endplate working its way into the disc until nucleus material can be extruded through this channel.

A dynamic disc-loading simulator was developed and validated to allow complex loading in order to provoke these kinds of failures. The requirements for this apparatus were to allow:

– Pure loads in all six degrees of freedom [flexion/extension (FE), lateral bending (LB), axial rotation (AR), laterolateral shear (SLL), anteroposterior shear (SAP), axial compression/decompression(AC)],
– Any load combination,
– High dynamic movements [±22.5° at 5 Hz (equal to 707°/s) for rotation and 100 mm/s translation],
– Angle/position control, and
– Loads up to 2 kN and 40 Nm.

After calibration and validation of this machine, a first test series was performed to investigate whether mechanical failure or even disc herniation can be provoked with healthy discs.

Methods

Disc-loading simulator

The general set-up of the dynamic disc-loading simulator is similar to the conventional material testing devices: a crosshead with two clamping blocks is guided by one column each (Fig. 1). The shafts are rigidly fixed to a baseplate that is mounted on a table. Overall dimensions of the machine are 1135 × 735 × 1655 mm (width × length × height) and weighs approximately 200 kg.

The crosshead is cardanic, allowing rotation about two independent axes. An *XYZ* table can produce independent translation along each of the three axes and provides the final rotational DOF. The construct was built primarily from aluminum to reduce weight and thus the inertial forces and moments. Non-moving parts of the frame (shafts, clamping blocks), that are crucial for stability, as well as some minor parts, were made from stainless steel.

Fig. 1 CAD drawing (*left*) and photograph (*right*) of dynamic disc-loading simulator with position of the coordinate system. *1* Crank handle, *2* swing, *3* counterweight, *4* angle transducer, *5* crosshead with clamping blocks, *6* specimen, *7* XYZ-table, *8* electric drive, *9* column, *10* six-component load cell, *11* path transducer (laser)
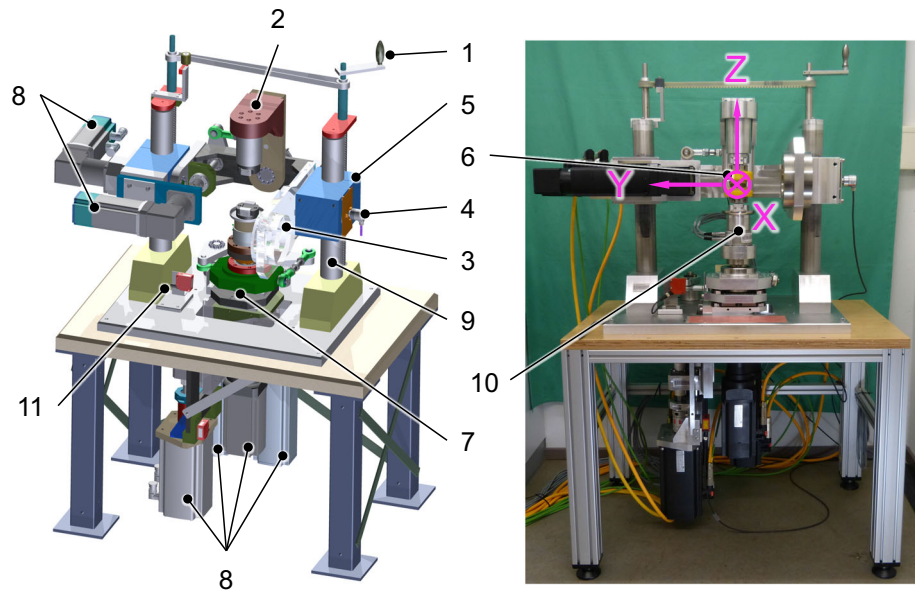
The specimen is aligned to the centre of the machine's coordinate system defined according to ISO 2631 and given by the position of the crosshead [44, 45] (Fig. 2).

Movement of the crosshead around the y axis produces flexion/extension and is driven directly. The swing (LB) is moved by a lever arm connected to the drive shaft of the motor by a cardan joint. AR is driven directly. Translation of the XYZ table in the x- (SAP) and y-directions (SLL) is coupled to the corresponding drive shaft by a lever arm. Translation in the z direction (AC) is transferred by a spindle drive (EPB 2505, THK, Ratingen, Germany) with a thread

Fig. 2 Detailed information about the movements applicable to the specimen and the machine's coordinate system

pitch of 5 mm. All translational movements are guided by linear bearings. The axes of all DOF are connected to the corresponding drive shaft by backlash-free couplings (JAW, Orbit, Wolfenbüttel, Germany). A counterweight was added to the crosshead to balance the FE axis.

All translational and rotational movements are driven by electric motors (Baumüller, Nürnberg, Germany) with a torque of 6–29 N m. To increase the maximum torque (29–224 Nm), gears (Neugart, Kippenheim, Germany) were added to all axes except the translation in z direction. A "b maXX 5000"-system power supply and driver (Baumüller, Nürnberg, Germany) is used.

The rotational stroke is $\pm22.5°$ for all axes and measured by angle transducers (Kübler, Villingen-Schwenningen, Germany) with a range of 45° and a resolution of 12 bit (0.01°). For safety reasons, the software limits were set to $\pm20.5°$. The translational stroke is ±7.5 mm for both the laterolateral and anteroposterior directions and ±19 mm for axial decompression/compression. Software limits were set to ±6.5 and ±17.5 mm, respectively. Three Laser sensors (ODSL 9, Leuze, Owen, Germany) with a resolution of 0.01 mm are used for measuring the translations.

Reaction forces up to ±10 kN (z axis) and ±2 kN (x-/y-axis) as well as moments up to 100 Nm (all axes) are measured by a six-component load cell (GTM, Bickenbach, Germany) placed directly beneath the specimen. Load and position are controlled by a Flextest-40-controller (MTS, Eden Prairie, MN, USA) that generates a ±10 V signal as input for the cascaded actuator controller (Fig. 3). Detailed information about all components used for the apparatus is given in Table 1.

Mounting of spinal motion segments with a height of up to 120 mm (including embedding) is possible. To align the
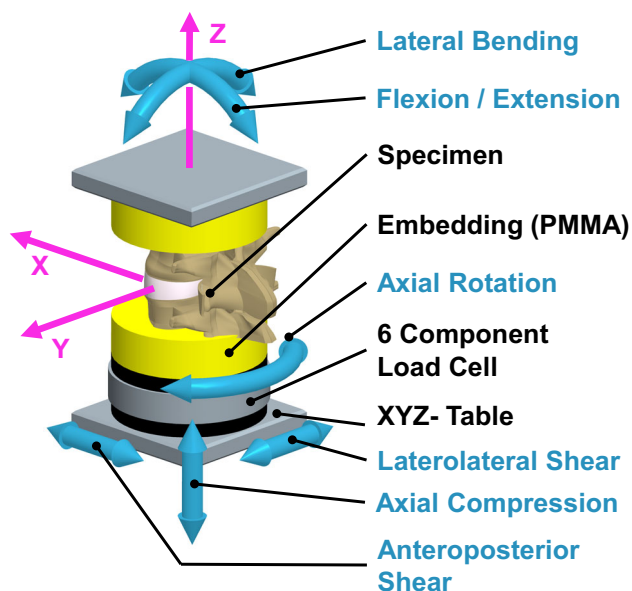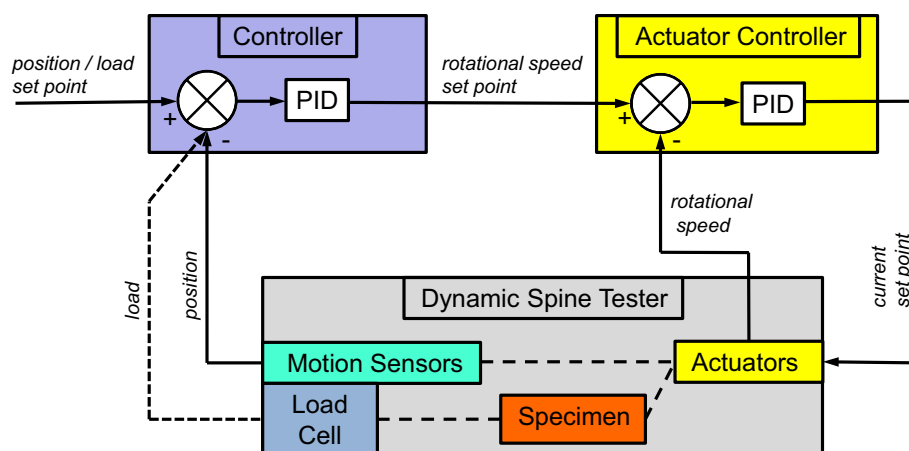
Fig. 3 Cascaded control loop configuration of the apparatus

Table 1 Detailed information about the main components used for the dynamic disc-loading simulator

Assembly	Component	Type	Notes	Company
Power source	Mains rectifier unit	BM 5031		Baumüller, Nürnberg, Germany
	Axis unit 1, 2	BM 5323		
	Axis unit 3, 4	BM 5331		
	Axis unit 5, 6	BM 5331		
Drive	*Engines*		*Gears*	
	Axis 1 (LB)	DSC045M64U20-5 (6.2 Nm)	WPLE80/90-i = 16	Baumüller, Nürnberg, Germany
	Axis 2 (FE)	DSC045M64U20-5 (6.2 Nm)	WPLE80/90-i = 32	Neugart, Kippenheim, Germany
	Axis 3 (AR)	DSC056S64U20-5 (10.5 Nm)	PLN 90-i = 12	
	Axis 4 (SAP)	DSD2-056LO64U-20-54 (14.0 Nm)	PLE 120/115-i = 16	
	Axis 5 (SLL)	DSD2-056LO64U-20-54 (14.0 Nm)	PLE 120/115-i = 16	
	Axis 6 (AC)	DSC071M64U20-5 (28.7 Nm)	–	
Control unit	Personal computer	HP Compaque 8200 elite		Hewlett Packard, Palo Alto, CA, USA
	Controller	Flextest 40	Mezzanine cards	MTS, Eden Prairie, MN, USA
			6 × 494.26	
			2 × 494.45	
			2 × 494.46	
Measuring devices	Six-component load cell		10 kN axial, 2 kN shear	GTM, Bickenbach, Germany
			100 Nm (all axes)	
	Angle transducer	Sendix 3651	0°–45°	Kübler, Villingen-Schwenningen, Germany
	Path transducer	ODSL 9/V6-100-S12	50–100 mm	Leuze, Owen, Germany

LB lateral bending, *FE* flexion/extension, *AR* axial rotation, *SAP* anteroposterior shear, *SLL* laterolateral shear, *AC* axial compression

centre of the intervertebral disc of the functional spinal unit (FSU) with the global coordinate system of the machine, the crosshead can be raised or lowered 100 mm using a crank handle. In addition, the swing height can be adjusted by 50 mm independent of the crosshead.

Operation of the machine and programming of arbitrarily complex loading protocols are done using commercial software (Basic Testware/Multipurpose Elite, MTS, Eden Prairie, MN, USA).

Position control analysis

A spring of defined mechanical properties (86/1/2, Knoerzer, Pfullingen, Germany) was used as surrogate of a real

motion segment to validate position control. The spring properties were chosen so that static forces and moments do not exceed 600 N and 50 N m, respectively. This ensured that typical in vitro loads are accessible. The ends of the spring (30 mm each) were embedded in poly-methylmethacrylate (PMMA, Technovit 3040, Heraeus Kulzer, Wehrheim, Germany). Flanges were screwed to the PMMA blocks so that the spring could be mounted in the dynamic disc-loading simulator. The middle of the spring was aligned with the origin of the machine's coordinate system in an unloaded condition (Fig. 4).

A sinusoidal waveform with an amplitude of $\pm 17°$ (FE, LB) and $\pm 8°$ (AR), respectively, was chosen for the target position. Translational amplitudes were ± 2 mm (SAP, SLL) and ± 3 mm (AC), respectively. All values were selected to stay well within the safe limits of the machine but still exceed typical physiological limits [44, 46–49].

Each of the six DOF was tested individually while the remaining axes were held stationary. Displacement was applied as a sine waveform at frequencies of 0.5, 1.75, and 3.0 Hz, simulating low, medium, and fast dynamic testing speeds typically used for in vitro tests. This resulted in a maximum angular speed of 320°/s and a maximum trans-lational speed of 36 mm/s. A total of 20 cycles were recorded of which the middle six median cycles were analysed for position error. Data were acquired at 100 Hz and analyzed using MATLAB (MATLAB 2013b, The MathWorks, Natick, MA, USA).

Ovine specimen study

Eight ovine lumbar motion segments were gathered from five healthy sheep aged between 3 and 5 years. The motion
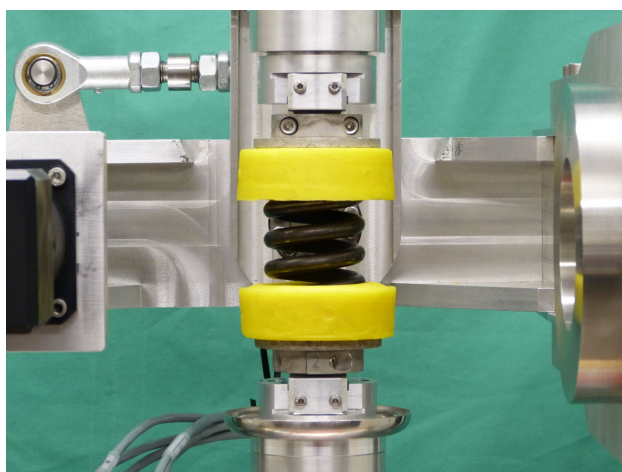

Fig. 4 Close-up photograph of the spring used as test specimen for position control analysis mounted in the dynamic disc-loading simulator

segments were immediately stored at -20 °C. Prior to testing, the specimens were thawed at 6 °C for 12 h. After dissection the vertebral bodies were cut in the middle of the transverse plane. To provide a clear view on the posterior anulus to observe a possible herniation during the tests, the posterior elements of the motion segments were removed. Care was taken to preserve anterior and posterior longitu-dinal ligaments. Screws were placed in the vertebral body of the motion segment to improve embedding in the PMMA (Technovit 3040, Heraeus Kulzer, Wehrheim, Germany). Flanges were screwed onto the PMMA to mount the specimens in the dynamic disc-loading simulator in an unloaded condition.

For preconditioning of the specimen, a compressive load of 130 N was applied for 15 min, simulating a typical spinal load of a standing sheep [50]. Testing was performed using the following protocol: 0°–12° flexion, 0°–9° right lateral bending, and 0°–4° right axial rotation combined with constant axial compression of 800 N typically occurring in vivo during dynamic activities [50]. The motions were applied cyclically with a frequency of 0.5 Hz. During the test, specimens were filmed from the posterior direction. Testing was stopped after 1200 cycles, which was deemed sufficient for the initiation and possible extrusion of nucleus material as found in a preliminary study with similar ovine specimens. Upon test completion, the discs were again frozen at -20 °C for a maximum of 4 weeks and thawed at 6 °C over night prior to the day of scanning. Imaging of the potential defects was performed in a dedicated 11.7 T small animal ultra-high field MRI system (UHF-MRI, BioSpec 117/16, Bruker Biospin, Ettlingen, Germany) using an experimental protocol (MR-method: FLASH, contrast: T1, Resolution: 75 µm iso-tropic, acquisition time: 9 h 25 min) [51]. All data were received with a 40 mm quadrature transmit/receive coil. Discs were scanned with no external load applied. Analysis of video documentation and scan images was done by visual inspection. Additionally, the scan images were used by specialized software (Avizo standard v5.6, FEI Visu-alization Sciences Group, Burlington, MA, USA) for seg-mentation and 3D-reconstruction of the disc and lesion volume.

Results

The new dynamic disc-loading simulator enables an arbi-trary combination of all six DOF. Loads of up to ± 10 kN in axial compression, ± 2 kN in both shear directions and moment up to 100 Nm around all axes can be applied (currently limited by the load cell). It allows high speeds of up to 707°/s and 100 mm/s.

Position control analysis

The actual position during motion typically displayed a consistent sinusoidal waveform at all frequencies, except for higher frequencies of both shear directions (Fig. 5).

Generally, the normalized error between target and actual position increased with rising testing frequency (Fig. 6). The highest median errors of 2.4 % were yielded by both shear directions (AP and LL) at 3.0 Hz (0.048 mm at 2 mm amplitude) where they also yielded the highest interquartile range (IQR) (SAP 4.4 %, SLL 6.1 %). The remaining four axes were almost similar with a median error of ≤ 2 % and an IQR of ≤ 2.4 % at all frequencies. The lowest error (median and IQR) was found for the FE-axis at 0.5 Hz (median 0.43 %/0.072°, IQR 0.40 %/0.068°).

During testing, the FE, LB, and AR moments typically reached ± 50, ± 50, and ± 30 Nm, respectively. Forces in SAP, as well as SLL direction were ± 250 N, while AC was ± 500 N.

Ovine specimen study

The first in vitro study in this dynamic testing machine showed that with the chosen complex motions failure of ovine discs can be produced in each specimen (Table 2). Three different kinds of lesions could be identified: four herniations, two protrusions, and two delaminations. Two modes of failure were observed when herniation or protrusion occurred: either anular failure (two cases) or endplate junction failure (four cases) (Table 2). Video documentation showed in three cases of herniation that the lesion developed within the first few cycles. One herniation was not visible because the sequestrum was covered by the posterior longitudinal ligament. Endplate lesions were generally noticed by a crackling noise while an anular lesion was barely audible. The sequestra were gradually pressed out and reached their maximum volume outside the
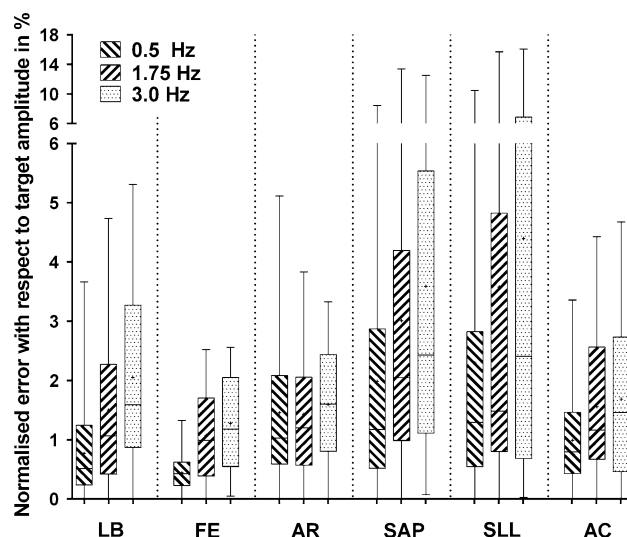

Fig. 6 Error between target and actual position with respect to the particular amplitude of the six axes (*LB* lateral bending, *FE* flexion/extension, *AR* axial rotation, *SAP* anteroposterior shear, *SLL* lateral-lateral shear, *AC* axial compression). The mean value is seen as a "+" sign

Table 2 Overview of the ovine specimen study's results

Specimen	Spinal segment	Failure location	Mode of failure
1	L5/6	Endplate	Prolapse
2	L1/2	Endplate	Prolapse[a]
3	L2/3	Anulus	Prolapse
4	L4/5	Endplate	Protrusion
5	L3/4	Anulus	Protrusion
6	L1/2	Endplate	Prolapse
7	L2/3	Anulus[b]	Delamination
8	L4/5	Anulus[c]	Delamination

[a] Covered by posterior longitudinal ligament

[b] Anterior

[c] Anterior and posterior

Fig. 5 Target and actual sine curves of typical (axial rotation, 1.75 Hz, *left*) and of highest error (laterolateral shear, 3.0 Hz, *right*). *Encircled areas* mark the effect of backlash
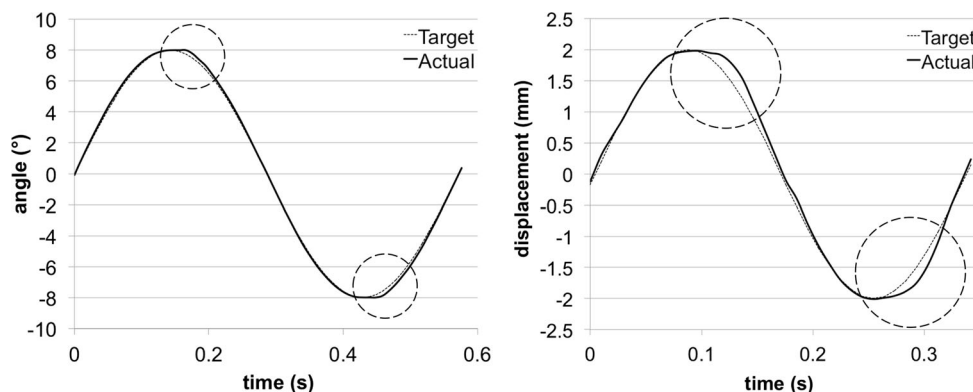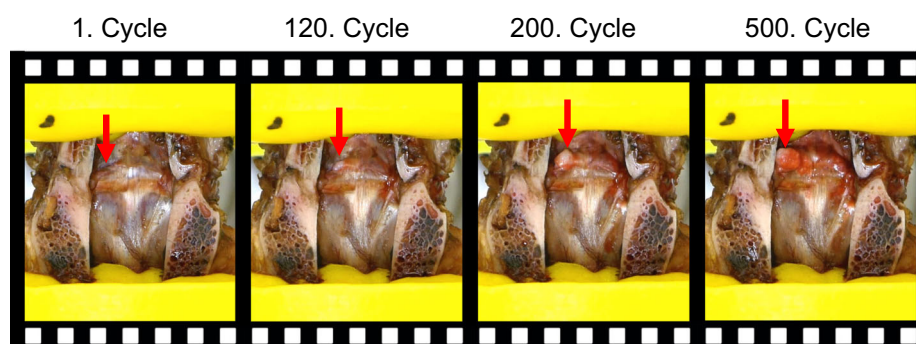
Fig. 7 Gradual development of a herniation. After 500 cycles the herniation does not increase further

anulus after a few cycles (one case) and after 500 cycles (two cases) (Fig. 7). In case of protrusion, a bulge on the left posterolateral side was noticed during testing. UHF-MRI scans revealed structural details of both failure patterns (Fig. 8). Failure was seen in the mid to left posterior part of the discs. UHF-MRI scans showed delaminations as areas of no signal inside the anulus.

Discussion

This paper introduces a new custom-designed dynamic disc-loading simulator with six DOF. It is suitable for most kinds of biomechanical testing of FSU and allows high speeds, which previously could only be attained by commercial robots, e.g. Kuka KR 16 (Kuka Robotik GmbH, Gersthofen, Germany). For in vitro tests with angular speeds <53°/s and displacement speeds <9.4 mm/s, the positioning accuracy can be specified as ≤0.08° and ≤0.026 mm, respectively. It does not reach the described high accuracy of the hexapod system by [41] but matches or exceeds the aforementioned commercial robotic system.

Position control analysis

The position control analysis demonstrated a general increase of error between target and actual position with increasing cycle frequency. This was to be expected, as in studies by Ding et al. [41] and Holsgrove et al. [32], since the required torque of the electric motors increases to the square with test frequency due to inertia of the moving parts, thus disturbing the control system.

For all test frequencies, higher errors were seen in each of the shear directions than in the remaining directions. When compared to the third translational DOF, the gears have a higher backlash (0.20° vs. 0.08°), there is additional mechanical laxity from the joint heads of the lever arms, and the 2 mm amplitude is equal to a rotational angle of the drive shaft of only about 20° (vs. 140°).

Although AR has the least moment of inertia of all rotational axes and a gear with the lowest backlash (<0.08°), it did not yield the highest accuracy. This can be explained by the smaller amplitude of ±8° used for the axis, since errors were normalised to amplitude.
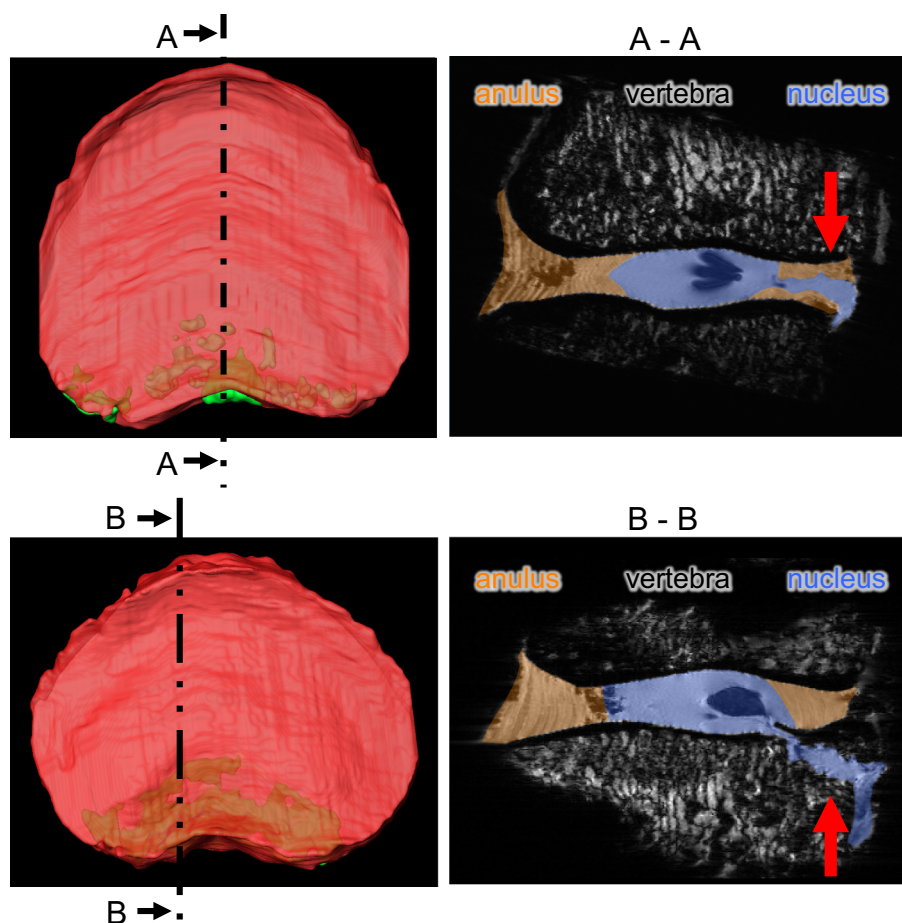
Ovine specimen study

Before using human specimens a first study was performed with ovine specimen applying a dynamic, complex loading protocol with four DOF. Four herniations and two protrusions, with either endplate junction failure or anular failure, were produced. The goal in this study was to show that it is possible to provoke disc failure under extreme conditions. Therefore, bending angles were chosen to be four times the values obtained by Wilke et al. [47] for the range of motion (ROM) of ovine lumbar FSUs at 7.5 Nm. Such failure could also be produced in vitro with an increased pressure by injecting gel into the nucleus [27]. Interestingly, the same ratio was found recently in a clinical study by Rajasekaran et al. [52] which showed that 117 of 181 patients (65 %) with herniations had an endplate junction failure.

The defects could nicely be visualized by the UHF-MRI. Unfortunately, it is not practical to scan all specimens also before testing because one scan with this high resolution requires about 10 h of scanning time and warms up the specimens which may have an effect on the failure mechanism. Therefore, only one of the specimens was scanned exemplarily prior to testing, which allowed comparison of the UHF-MRI images after failure with the status before. This specimen did not show any indications of defects. Previous histologic studies of sheep from the same source aged between 3 and 5 years also showed no marked pre-existing defects [53].

Even though only eight specimens were used, it seems that there is a tendency toward endplate junction failure (4 times) over anular failure (2 times). This implicates the bone, rather than the disc, as the structure primarily susceptible to damage.

Usually, bone mineral density (BMD) of ovine vertebral bodies is 6.5 times higher than human specimens [54, 55]. However, it is not known how the BMD affects the mode of failure. Since a similar trend was present in the current

Fig. 8 Reconstructed volume of a disc (*red*) and lesions (*green*) in craniocaudal view (*left*). Sagittal 11.7 T MRI section in the area of the lesion (*right*). L1/2 anular lesion (*top*) and L4/5 endplate lesion (*bottom*). For better visibility nucleus and anulus are highlighted in color

study, it may be concluded that ovine specimens, even having a higher BMD, is a useful failure model of the human disc.

A recent ovine in vitro study by Wade et al. [26], using an apparatus previously introduced by Adams et al. [56], is more comparable to the test conducted in the present study since flexion (10°) was achieved by compression (approximately 10 kN). Wade et al. [26] only found anular failures and endplate fractures, but no endplate junction failures. It may therefore be concluded that the biomechanical approach of load application has an important influence on the mode of failure. Therefore, further investigation in this area is imperative.

While mechanical fixtures integrated into uni- or biaxial testing machines are used for a specific load scenario and thereby limited in their design, the dynamic disc-loading simulator presented allows any type of load combination, thus rendering it highly versatile.

The apparatus is prepared for several enhancements. A water bath can easily be added when testing for several hours. The usage of an external motion capture system as was previously done by [57] is possible since the view of the specimen is unobstructed. Intradiscal pressure measurements can also be conducted and are automatically synchronized with load and displacement measurements by connecting the pressure sensors to the analog input of the Flextest-40-controller. Furthermore, a second load cell can be installed on the cranial side of the specimen if desired.

A limitation of the apparatus is the maximum angular speed about the FE axis; this motion direction does not reach the desired value of 707°/s but rather only 400°/s, owing to the fact that a balancing weight was added. Currently, load control is available for axial compression only. Implementation of further load controlled DOF is under investigation. Another limitation is that any displacement results in reaction forces, dependent upon the specimen's stiffness typically seen in dynamic in vitro tests. A possible solution would be load- or hybrid control, however, load control for dynamic testing is technically challenging.

Conclusions

A new, custom-designed, electromechanical, 6-DOF dynamic disc-loading simulator was developed and validated. It is highly versatile and expandable if desired. This

device provides new possibilities for fundamental spine biomechanics research. An initial study on ovine specimens showed that herniation can be provoked with complex loading. Experiments in this new dynamic disc-loading simulator will improve understanding of the initiation of intervertebral disc lesions, especially in human disc specimens. This device is now ready to perform many studies on discs with different degrees of degeneration from different regions of the spine to differentiate between different load scenarios or other parameters such as number of load cycles or velocity. The findings from this first experiment form the foundation for future experiments to find the critical load cases.

These findings may have a great impact on the credibility and confidence of medical court expert testimony. Another notable application includes implant failure testing (subsidence of cages, dislocation of nucleus implants or disc prosthesis, failure of anulus sealing methods, pedicle screw loosening, etc.) under complex physiological conditions or following ASTM or ISO standards.

Compliance with ethical standards

Conflict of interest The authors have no conflicts of interest to disclose.

References

1. Kanna RM, Shetty AP, Rajasekaran S (2014) Patterns of lumbar disc degeneration are different in degenerative disc disease and disc prolapse magnetic resonance imaging analysis of 224 patients. Spine J 14(2):300–307. doi:10.1016/j.spinee.2013.10.042

2. Andersson G (1997) Epidemiology of spinal disorders. In: Frymoyer JW, Ducker TB, Hadler NM, Kostuik JP, Weinstein JN, Whitecloud TSI (eds) The adult spine: principles and practice. Raven Press, New York, pp 93–141

3. Federal Statistical Office of Germany (2012) Health monitoring information system—diagnostic data (ICD 10: M51.0-51.2). http://www.gbe-bund.de

4. Postacchini F, Cinotti G (1999) Etiopathogenesis. In: Postacchini F (ed) Lumbar disc herniation. Springer, Wien, pp 151–164, 629

5. White AAI, Panjabi MM (1990) Clinical biomechanics of the spine. J.B. Lippincott Company, Philadelphia

6. Vergroesen PP, Kingma I, Emanuel KS, Hoogendoorn RJ, Welting TJ, van Royen BJ, van Dieen JH, Smit TH (2015) Mechanics and biology in intervertebral disc degeneration: a vicious circle. Osteoarthr Cartil OARS Osteoarthr Res Soc 23(7):1057–1070. doi:10.1016/j.joca.2015.03.028

7. Virgin WJ (1951) Experimental investigations into the physical properties of the intervertebral disc. J Bone Joint Surg Br 33(4):607–611

8. Hirsch C (1955) The reaction of intervertebral discs to compression forces. J Bone Joint Surg Am 37(6):1188–1196

9. Brown T, Hansen RJ, Yorra AJ (1957) Some mechanical tests on the lumbosacral spine with particular reference to the intervertebral discs—a preliminary report. J Bone Joint Surg Am 39(5):1135–1164

10. Hardy WG, Lissner HR, Webster JE, Gurdjian ES (1958) Repeated loading tests of the lumbar spine; a preliminary report. Surg Forum 9:690–695

11. Roaf R (1960) A Study of the mechanics of spinal injuries. J Bone Joint Surg Br 42(4):810–823

12. Farfan HF, Cossette JW, Robertson GH, Wells RV, Kraus H (1970) The effects of torsion on the lumbar intervertebral joints: the role of torsion in the production of disc degeneration. J Bone Joint Surg Am 52(3):468–497

13. Lin HS, Liu YK, Adams KH (1978) Mechanical response of the lumbar intervertebral joint under physiological (complex) loading. J Bone Joint Surg Am 60(1):41–55

14. Wilder DG, Pope MH, Frymoyer JW (1982) Cyclic loading of the intervertebral motion segment. In: Hansen EW (ed) Proceedings of the tenth annual northeast bioengineering conference, Dartmouth College, Hanover, New Hampshire, March 15–16, 1982. New York, IEEE, pp 9–11, 356

15. Wilder DG, Pope MH, Frymoyer JW (1988) The biomechanics of lumbar disc herniation and the effect of overload and instability. J Spinal Disord 1(1):16–32

16. Liu YK, Njus G, Buckwalter J, Wakano K (1983) Fatigue response of lumbar intervertebral joints under axial cyclic loading. Spine 8(8):857–865

17. Liu YK, Goel VK, Dejong A, Njus G, Nishiyama K, Buckwalter J (1985) Torsional fatigue of the lumbar intervertebral joints. Spine 10(10):894–900

18. Adams MA, Hutton WC (1981) The relevance of torsion to the mechanical derangement of the lumbar spine. Spine 6(3):241–248

19. Adams MA, Hutton WC (1982) The mechanics of prolapsed intervertebral disc. Int Orthop 6(4):249–253

20. Adams MA, Hutton WC (1982) Prolapsed intervertebral disc. A hyperflexion injury 1981 Volvo Award in Basic Science. Spine 7(3):184–191

21. Adams MA, Hutton WC (1983) The effect of fatigue on the lumbar intervertebral disc. J Bone Joint Surg Br 65(2):199–203

22. Adams MA, Hutton WC (1985) Gradual disc prolapse. Spine 10(6):524–531

23. Callaghan JP, McGill SM (2001) Intervertebral disc herniation: studies on a porcine model exposed to highly repetitive flexion/extension motion with compressive force. Clin Biomech (Bristol, Avon) 16(1):28–37

24. Drake JDM, Aultman CD, McGill SM, Callaghan JP (2005) The influence of static axial torque in combined loading on intervertebral joint failure mechanics using a porcine model. Clin Biomech (Bristol, Avon) 20(10):1038–1045

25. Marshall LW, McGill SM (2005) The role of axial torque in disc herniation. Clin Biomech (Bristol, Avon) 25(1):6–9

26. Wade KR, Robertson PA, Thambyah A, Broom ND (2014) How healthy discs herniate: a biomechanical and microstructural study investigating the combined effects of compression rate and flexion. Spine (Phila Pa 1976) 39(13):1018–1028. doi:10.1097/BRS.0000000000000262

27. Veres SP, Robertson PA, Broom ND (2010) ISSLS prize winner: how loading rate influences disc failure mechanics: a microstructural assessment of internal disruption. Spine (Phila Pa 1976) 35(21):1897–1908. doi:10.1097/BRS.0b013e3181d9b69e

28. Kelly BP, Bennett CR (2013) Design and validation of a novel Cartesian biomechanical testing system with coordinated 6DOF real-time load control: application to the lumbar spine (L1-S, L4-L5). J Biomech 46(11):1948–1954. doi:10.1016/j.jbiomech.2013.05.008

29. Chang TS, Cheng CW, Wang CS, Chen HY, Chang JH (2009) A new multi-direction tester for evaluation of the spinal biomechanics. J Med Biol Eng 29(1):7–13

30. Chung SM, Teoh SH, Tsai KT, Sin KK (2002) Multi-axial spine biomechanical testing system with speckle displacement instrumentation. J Biomech Eng T Asme 124(4):471–477. doi:10.1115/1.1493803

31. Crawford NR, Brantley AG, Dickman CA, Koeneman EJ (1995) An apparatus for applying pure nonconstraining moments to spine segments in vitro. Spine (Phila Pa 1976) 20(19):2097–2100

32. Holsgrove TP, Gheduzzi S, Gill HS, Miles AW (2014) The development of a dynamic, six-axis spine simulator. Spine J 14(7):1308–1317. doi:10.1016/j.spinee.2013.11.045

33. Panjabi MM (2007) Hybrid multidirectional test method to evaluate spinal adjacent-level effects. Clin Biomech (Bristol, Avon) 22(3):257–265. doi:10.1016/j.clinbiomech.2006.08.006

34. Panjabi MM, Krag MH, Goel VK (1981) A technique for measurement and description of three-dimensional six degree-of-freedom motion of a body joint with an application to the human spine. J Biomech 14(7):447–460

35. Stokes IA, Gardner-Morse M, Churchill D, Laible JP (2002) Measurement of a spinal motion segment stiffness matrix. J Biomech 35(4):517–521

36. Strube P, Tohtz S, Hoff E, Gross C, Perka C, Putzier M (2010) Dynamic stabilization adjacent to single-level fusion: part I. Biomechanical effects on lumbar spinal motion. Eur Spine J 19(12):2171–2180. doi:10.1007/s00586-010-1549-9

37. Tan JS, Singh S, Zhu QA, Dvorak MF, Fisher CG, Oxland TR (2008) The effect of cement augmentation and extension of posterior instrumentation on stabilization and adjacent level effects in the elderly spine. Spine (Phila Pa 1976) 33(25):2728–2740. doi:10.1097/BRS.0b013e318188b2e4

38. Wilke HJ, Claes L, Schmitt H, Wolf S (1994) A universal spine tester for in vitro experiments with muscle force simulation. Eur Spine J 3(2):91–97

39. Fujie H, Mabuchi K, Woo SL, Livesay GA, Arai S, Tsukamoto Y (1993) The use of robotics technology to study human joint kinematics: a new methodology. J Biomech Eng 115(3):211–217

40. Hurschler C, Pott L, Gossé F, Wirth C (2005) Sensor-guided robotic spine motion-segment biomechanical testing: Validation against the pure moment apparatus. In: Transactions of the 51st annual meeting of the Orthopaedic Research Society, Washington DC

41. Ding BY, Stanley RM, Cazzolato BS, Costi JJ (2011) Real-time FPGA Control of a Hexapod Robot for 6-DOF Biomechanical Testing. IEEE Ind Elec

42. Lawless IM, Ding B, Cazzolato BS, Costi JJ (2014) Adaptive velocity-based six degree of freedom load control for real-time unconstrained biomechanical testing. J Biomech 47(12):3241–3247. doi:10.1016/j.jbiomech.2014.06.023

43. Schmidt H, Kettler A, Heuer F, Simon U, Claes L, Wilke HJ (2007) Intradiscal pressure, shear strain, and fiber strain in the intervertebral disc under combined loading. Spine (Phila Pa 1976) 32(7):748–755. doi:10.1097/01.brs.0000259059.90430.c2

44. ISO 2631-1:1997 Mechanical vibration and shock—evaluation of human exposure to whole-body vibration. Part 1: General requirements

45. Wilke HJ, Wenger K, Claes L (1998) Testing criteria for spinal implants: recommendations for the standardization of in vitro stability testing of spinal implants. Eur Spine J 7(2):148–154

46. Wang S, Park WM, Kim YH, Cha T, Wood K, Li G (2014) In vivo loads in the lumbar L3-4 disc during a weight lifting extension. Clin Biomech (Bristol, Avon) 29(2):155–160. doi:10.1016/j.clinbiomech.2013.11.018

47. Wilke HJ, Kettler A, Claes LE (1997) Are sheep spines a valid biomechanical model for human spines? Spine (Phila Pa 1976) 22(20):2365–2374

48. Wilke HJ, Krischak S, Claes L (1996) Biomechanical comparison of calf and human spines. J Orthop Res 14(3):500–503. doi:10.1002/jor.1100140321

49. Wilke HJ, Geppert J, Kienle A (2011) Biomechanical in vitro evaluation of the complete porcine spine in comparison with data of the human spine. Eur Spine J 20(11):1859–1868. doi:10.1007/s00586-011-1822-6

50. Reitmaier S, Schmidt H, Ihler R, Kocak T, Graf N, Ignatius A, Wilke HJ (2013) Preliminary investigations on intradiscal pressures during daily activities: an in vivo study using the merino sheep. PLoS ONE 8(7):e69610. doi:10.1371/journal.pone.0069610

51. Berger-Roscher N, Galbusera F, Rasche V, Wilke H-J (2015) Intervertebral disc lesions: visualisation with ultra-high field MRI at 11.7 T. Eur Spine J 24(11):2488–2495. doi:10.1007/s00586-015-4146-0

52. Rajasekaran S, Bajaj N, Tubaki V, Kanna RM, Shetty AP (2013) ISSLS Prize winner: The anatomy of failure in lumbar disc herniation: an in vivo, multimodal, prospective study of 181 subjects. Spine (Phila Pa 1976) 38(17):1491–1500. doi:10.1097/BRS.0b013e31829a6fa6

53. Reitmaier S, Kreja L, Gruchenberg K, Kanter B, Silva-Correia J, Oliveira JM, Reis RL, Perugini V, Santin M, Ignatius A, Wilke HJ (2014) In vivo biofunctional evaluation of hydrogels for disc regeneration. Eur Spine J 23(1):19–26. doi:10.1007/s00586-013-2998-8

54. Campbell AW, Bain WE, McRae AF, Broad TE, Johnstone PD, Dodds KG, Veenvliet BA, Greer GJ, Glass BC, Beattie AE, Jopson NB, McEwan JC (2003) Bone density in sheep: genetic variation and quantitative trait loci localisation. Bone 33(4):540–548

55. Yoganandan N, Pintar FA, Stemper BD, Baisden JL, Aktay R, Shender BS, Paskoff G, Laud P (2006) Trabecular bone density of male human cervical and lumbar vertebrae. Bone 39(2):336–344. doi:10.1016/j.bone.2006.01.160

56. Adams MA, Hutton WC, Stott JR (1980) The resistance to flexion of the lumbar intervertebral joint. Spine (Phila Pa 1976) 5(3):245–253

57. Heineck J, Haupt C, Werner K, Rammelt S, Zwipp H, Wilke HJ (2010) Fracture models in the lumbar sheep spine: a biomechanical investigation. J Orthop Res 28(6):773–777. doi:10.1002/jor.21057